Pneumatic Brake Control for Precision Stopping of Heavy-Duty Vehicles

Fanping Bu+, Han-Shue Tan

Abstract

Precision stopping is an important automated vehicle control function that is critical in applications such as precision bus docking, automated truck or bus fueling, as well as automatic intersection or toll booth stopping. The initial applications of this technology are most likely to be applied to heavy-duty vehicles such as buses or trucks. Such applications require specific attention to brake control since the characteristics of a typical pneumatic brake system of a heavy vehicle is inherently nonlinear with large uncertainties. The feasibility of providing a smooth precision stopping brake control based on a conventional pneumatic brake system has not yet been demonstrated. This paper describes the precision stopping problem, verifies the pneumatic brake model, details the Indirect Adaptive Robust Control (IARC) design for a pneumatic brake system, and reports the successful implementation of a bus precision docking demonstration.

Index Terms

Precision Stopping, Pneumatic Brake Model, Backstepping Control, Indirect Adaptive Robust Control

I. Introduction

Vehicle control has been studied for many years in areas such as automated highway system (AHS) [1], vehicle stability control [2], and driver assistance. Some research results have been applied to support real-world driver assistance applications such as adaptive cruise control, roll-stability control and parking assistance. However, several good candidates for early adaptations of a ”true” automation are applications on heavy-duty vehicles [3], [4] such as automated bus

The authors are with the California PATH, University of California at Berkeley, 1357 S. 46th Street, Richmond, CA 94804. (email: fanping@path.berkeley.edu, hstan@path.berkeley.edu)

rapid transits [5], automated truck/container yard operations [6], heavy-duty vehicle maintenance automation, as well as automatic operations for specialty vehicles such as automated snow removal [7]. Many such operations require the stopping system to automatically control the heavy-duty vehicle to stop smoothly and precisely in a consistent way equal to or greater than those from an experienced operator. Docking bus precisely, backing automated trucks and trailers onto a platform, fueling automated trucks or buses, as well as stopping automatically at intersections are some examples.

Controlling a vehicle to a complete stop is one of the longitudinal vehicle control functions. In particular, it is essential that a bus or a truck can apply a very fine brake control in order to stop at a designated location exactly. Most of the prior research on vehicle longitudinal controls focuses on the areas of high speed platooning [8], [9], adaptive cruise control [10] and string stability [11]. The works related to vehicle stopping or fine brake control are limited to the Anti-lock Brake System (ABS) [12], vehicle stability [13] or passenger cars equipped with a hydraulic brake [14]. The design of a precision stopping controller for a heavy-duty vehicle has not been fully examined and deserves a closer investigation.

Furthermore, most buses and trucks today are equipped with pneumatic brake systems that use compressed air as the energy medium. From the control point of view, the pneumatic brake system has several characteristics that make the control design difficult. First, the compressibility of air introduces a large time delay, which limits system bandwidth. Second, the dynamics of the pneumatic brake system are highly nonlinear because of the nonlinear pressure/air flow relationship. Third, the pneumatic brake system, when coupled with heavy-duty vehicle longitudinal dynamics, has large uncertainties. Many factors contribute to these uncertainties: changing supply pressures due to brake release, increasing brake temperature due to frequent braking, brake wear, large load variation and changing road surface conditions due to rain or snow. Even with all those potential disadvantages, it is still desirable that the automatic brake control system uses the existing pneumatic brake as the primary means of stopping control either by tabbing into the braking control commands or including an add-on actuator. Using the existing pneumatic brake system allows the automated vehicle to maintain all its manual braking capabilities. The ability to remain ”dual use” is one of the common requirement preferences for the early automation deployment requirements. Relevant work on the pneumatic brake in literature focuses mainly in the areas of ABS [12], [15] and fault diagnosis [16]. A comprehensible brake model was

developed for diagnosis purposes in [16], however it was too complex for control design. In [9], [17], a simplified linear model with time delay is developed based on input/output relationship, and is used for high speed longitudinal control. Recent literatures that relate to the subject of pneumatic actuator controls (e.g. for robot motion control) [18] suggest that nonlinear model based control laws achieve superior performance over their linear counterparts. Accurate yet tractable nonlinear models for the pneumatic brake system and associated high performance nonlinear model-based control design for automated vehicles has not been fully investigated yet.

The purposes of this paper are to provide a detailed analysis on the precision stopping problems of heavy-duty vehicles using conventional pneumatic brake systems, and to demonstrate its feasibility under a realistic application environment. To address the difficulties of control design for pneumatic brake system, a simplified nonlinear model will be identified for the control design; a control synthesis strategy based on nonlinear models, Indirect Adaptive Robust Control approach (IARC) [19], [20], will be used in this paper. A baseline robust controller will be synthesized to address the model uncertainties associated with the brake system. Parameter adaptation will be used to reduce the model uncertainties introduced by vehicle loads, brake characteristics and tire/road surface conditions. An indirect adaptive control technique will be employed to decouple the parameter adaptation design from the feedback control design in order to achieve accurate parameter estimation performance. An accurate parameter estimation can be crucial at the final stop phase of the precision stopping, when the brake system is under open loop control without precise position and velocity measurement.

The application example presented in this paper is the ”precision stopping” of a 40 foot CNG bus for the Bus Precision Docking public demonstrations at Washington, D.C. in 2003. These precision docking demonstrations consistently achieved 1 cm lateral and 15 cm longitudinal accuracies. Such high docking accuracies would allow fast loading and unloading of passengers similar to that of trains and greatly reduce the stress of manual docking in a high throughput Advance Bus Rapid Transit system [5]. Precision docking and stopping can also be a useful component for the concept of an Advanced Maintenance Station [3], where quick fuel fill-up, washing, and maintenance can be automatically performed at the end of each run.

This paper is organized as follows: Section II defines the precision stopping problem for heavy-duty vehicles; Section III describes and verifies the pneumatic brake model; Section IV details the design of the IARC brake controller; the successful implementation of a bus precision

docking demonstration is discussed in Section V; Section VI concludes the paper.

II. Precision Stopping Problem Formulation and System Design

Two different approaches can be used to formulate the precision stopping problem. One approach is the trajectory following. A desired trajectory is synthesized according to the initial vehicle speed and position, and the final stop position. The controller is designed so that vehicle will follow the desired trajectory with appropriate brake command. The second approach is to dynamically synthesize a desired deceleration based on the vehicle's speed and remaining distance to the designated stop location. Brake servo command is generated to follow the desired deceleration. Since the main purpose of this paper is to investigate the feasibility of precision stopping with pneumatic brake system, the more intuitive and direct approach-, the trajectory following approach, is adopted. The precision stopping problem of vehicle can be formulated into a trajectory following problem as follows:

Given an initial vehicle speed v_0, synthesize a brake control command u such that the vehicle follows the synthesized deceleration profile $x_{ld}(t)$ and stops at the desired location $x_{1d}(T)$ with a maximum error e_{max} and with desired smoothness represented by bounded deceleration a_{max} and jerk j_{max} (such as suggested in [21], [22]).

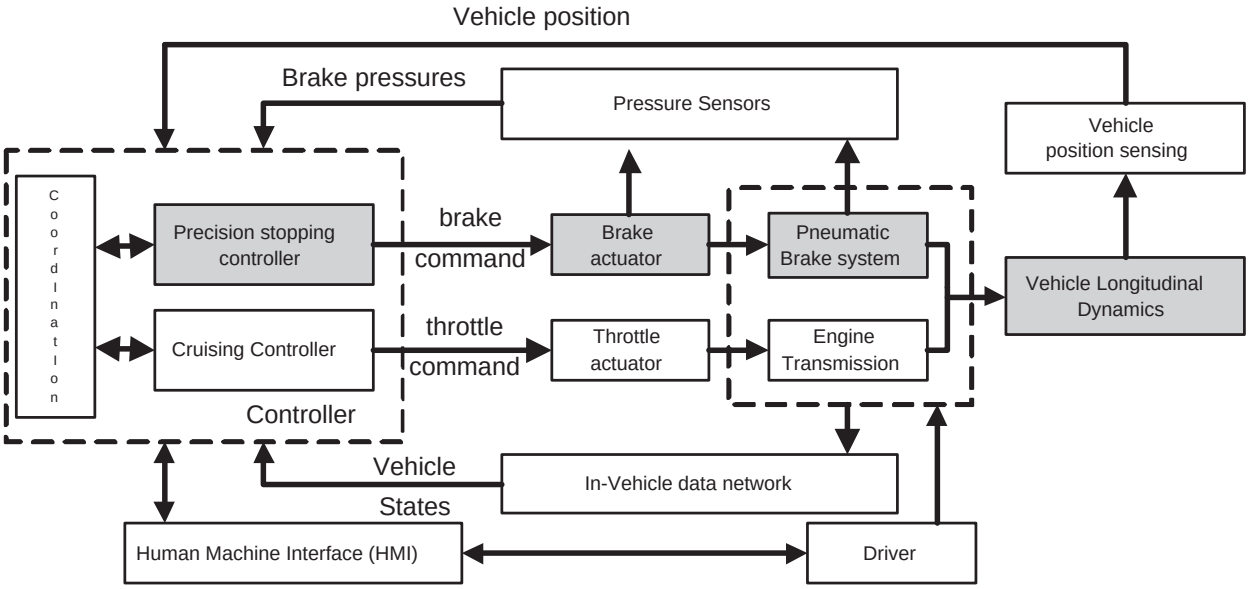

Fig. 1. Schematics of a precision stopping system

Fig. 1 shows a general schematics of a precision stopping system based on a pneumatic brake system. The whole system includes cruise speed control, precision stopping control, coordination control and human machine interface (HMI). This paper focuses only on the blocks directly related to the precision stopping control (shaded blocks in Fig. 1): precision stopping controller, brake actuator, pneumatic brake system, and vehicle longitudinal dynamics during braking. Precision stopping controller synthesizes a deceleration trajectory and the brake control command according to the sensor information. Sensor information could be air pressures inside the pneumatic brake system, vehicle states (e.g. vehicle speed, gear position and engine speed) and vehicle position. Most vehicle states are available through in-vehicle data network (e.g. J1939 bus for heavy-duty vehicles). Vehicle position can be obtained from GPS, magnetic markers or transbounders buried underground, video cameras and/or vehicle speed integration.

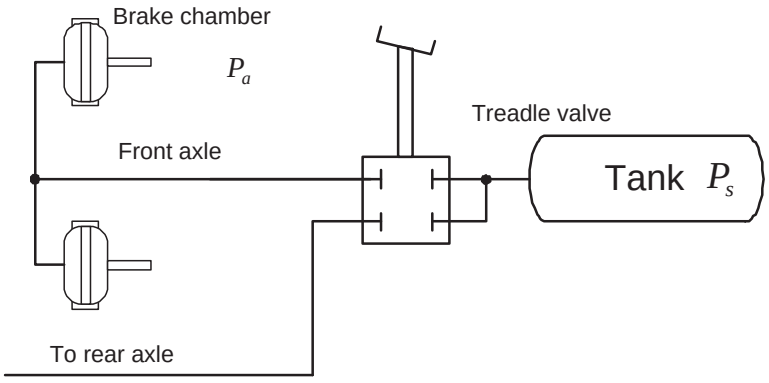

Fig. 2. General schematics of pneumatic brake system

Fig. 2 shows the pneumatic loop of a typical heavy-duty vehicle air brake system. When the driver presses the brake pedal, the treadle valve is opened and compressed air flows from air tank to the brake chambers. The brake chamber is a diaphragm actuator which converts the energy of air pressure to the mechanical force. Such mechanical force is transmitted to the brake pad through the push rod and brake cam. Brake force is generated by the friction between the brake pad and brake drum. Air is released to the atmosphere when the driver depresses the brake pedal. The compressor is turned on to recharge the air tank when the air tank pressure is below certain level due to air release,

A brake actuator receives brake control command and ”actuates” the pneumatic brake system

so that the desired brake force can be delivered to slow down the vehicle. The brake actuator can be designed in many ways, but it is desirable that it does not interfere with manual operation because of safety concerns. In [23], an electrical motor is added to control the brake pedal position. This method does not modify the original brake system, but it often introduces additional dynamics and nonlinearities such as brake pedal stiction. In [24], a ”brake by wire” system (WABCO electronic braking system (EBS)) is used to replace the original air brake system. Inspired by the WABCO EBS design, this paper proposed a general ”brake by wire” system

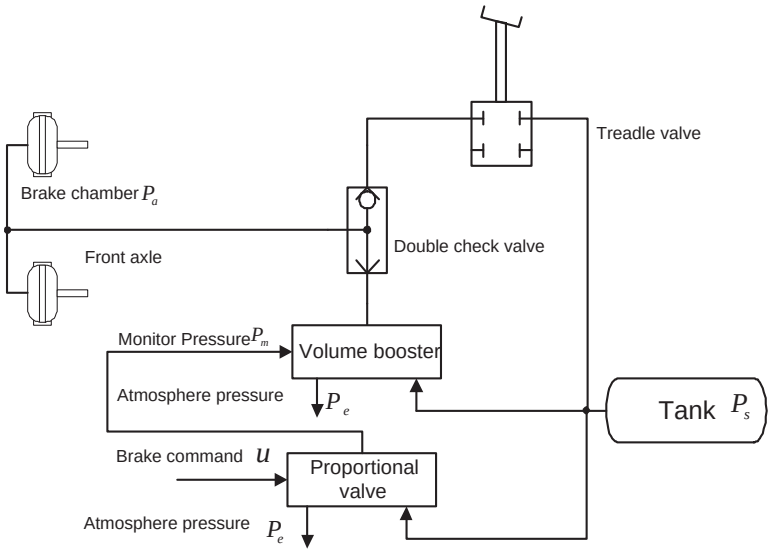

Fig. 3. Schematic of front axle brake actuator (rear axle is similar)

consisting of ”off-the-shelf” pneumatic valves, as shown in Fig 3. The design enables automatic control of the pneumatic brake system and maintains the full integrity of the original air brake system. A computer-controlled proportional pneumatic valve is installed between the air tank and brake chamber. In order to achieve a quick apply and release response, a volume booster is added into the loop to supply the air volume for a fast brake apply and release. Double check valve is used to ensure that the original air brake system will still be able to be operated by the brake pedal with the added hardware.

III. Dynamic Vehicle and Brake Model

In this section, dynamic models for the brake actuator and the pneumatic brake system, as well as the vehicle longitudinal braking motion, will be developed. Model reductions are made

to facilitate controller design. Experimental data using the demonstration setup (described in Section V) together with the physical explanations are used to justify the model reductions and to illustrate the accuracy of the resultant model.

A. Modeling of brake actuator

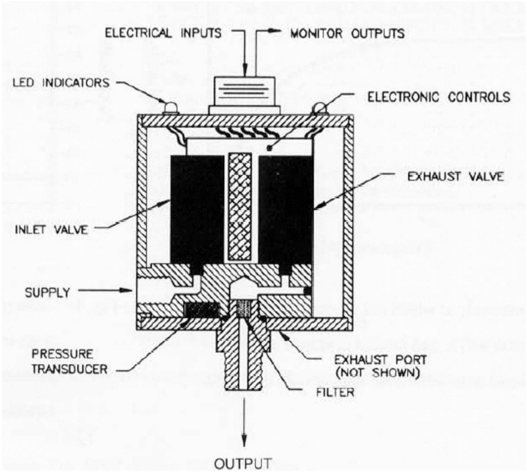

Fig. 4. Schematic of a proportional pneumatic valve (Proportion-Air's QB1 valve)

As shown in Fig. 3 and Fig. 4, a proportional pneumatic valve is used in the brake actuator. Output pressure (monitor pressure P_m) is proportional to the electrical command input u. P_m is controlled by two solenoid valves inside the proportional valve. One such solenoid valve functions as the inlet valve, the other as the exhaust. P_m is measured by a pressure transducer internal to the proportional valve which provides a feedback signal to the electronic controls. Internal electronic control of the proportional valve serves as a closed pressure loop to maintain linear relation between the input command signal u and output pressure P_m. Because of the closed pressure loop and a very small air volume between the proportional valve's output port and the pilot input port of the volume booster, the dynamics of the proportional pneumatic valve can be approximated by a linear system. For example, a frequency sweeping experiment is conducted to obtain frequency response from input command signal u_v to monitor pressure P_m for the Proportion-Air's QB1 valve in our experimental setup. The frequency response for

this specific valve as shown in Fig. 5 can be fitted with a first order transfer function:

$$\frac{P_m(s)}{U_v(s)} = \frac{3.4659}{s+3.7474} \tag{1}$$

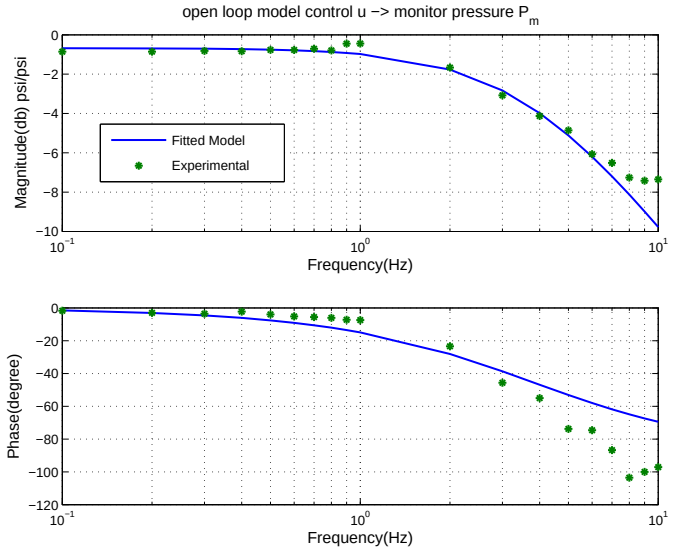

Fig. 5. Frequency response of a proportional pneumatic valve (Proportion-Air's QB1 valve)

Alone, especially when the brake is releasing, a typical small proportional pneumatic valve cannot provide enough air flow. Therefore, a volume booster is often mounted to improve response time. In our experimental setup, the Proportion-Air R series, as shown in Fig. 6, is used. The volume booster is an air-piloted, diaphragm-operated, self-venting regulator. Output pressure from the proportional valve is used as the pilot input pressure. The diaphragm is balanced by the input pilot pressure signal and the output pressure. Any difference between the pilot input pressure and the output pressure will move the diaphragm and open either the supply valve or exhaust valve so that the output pressure follows pilot input pressure. The air flow inside the volume booster can be described as, ideally, compressible gas passing through an orifice. As suggested in [25], we assume that

- Air is ideal
- Air density is uniform in pipe and brake chamber
- Air in pneumatic circuit is isentropic process

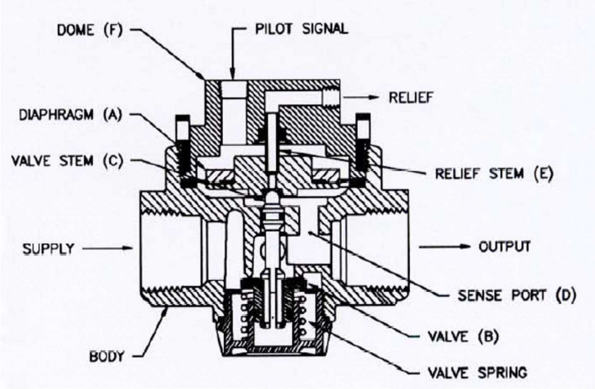

Fig. 6. Schematics of a volume booster (Proportion-Air R series)

The air mass flow rate that passes through the volume booster can be expressed by:

$$\dot{m} = \begin{cases} C_s A_s(P_m, P_a) P_s \sqrt{\frac{2}{RT}} f(\frac{P_a}{P_s}) & r_s P_m \geq P_a(supply) \\ -C_e A_e(P_m, P_a) P_a \sqrt{\frac{2}{RT}} f(\frac{P_{air}}{P_a}) & r_s P_m < P_a(release) \end{cases} \tag{2}$$

where $\dot{m}$ is the air mass flow rate that passes through the orifice, C_s and C_e are the orifice discharge coefficients that can be determined as in [15], P_s is the air pressure inside the supply tank, P_a is the air pressure inside the brake chamber, P_{air} is the atmosphere pressure, $A_s(P_m, P_a)$ and $A_e(P_m, P_a)$ are the effective orifice areas which are functions of the pilot input pressure P_m and output brake chamber pressure P_a, R is the ideal gas constant, r_s is the effective area ratio between the two sides of the diaphragm, and T is the temperature. The piecewise continuous flow function $f(\alpha)$ is defined by:

$$f(\alpha) = \begin{cases} \sqrt{\frac{\gamma}{\gamma-1}(\alpha^{\frac{2}{\gamma}} - \alpha^{\frac{\gamma+1}{\gamma}})} & \alpha_c \leq \alpha \leq 1 \\ \sqrt{\frac{\gamma}{\gamma+1}(\frac{2}{\gamma+1})^{\frac{2}{\gamma-1}}} & 0 \leq \alpha < \alpha_c \end{cases} \tag{3}$$

where α is the pressure ratio, γ is the ratio of special heat and α_c is the critical pressure ratio given by $\alpha_c = (\frac{2}{\gamma+1})^{\frac{\gamma}{\gamma-1}}$.

Fig. 7 shows the static response of the brake system in the experimental setup. The effective orifice areas are proportional to the pressure difference between P_m and P_a as shown in the

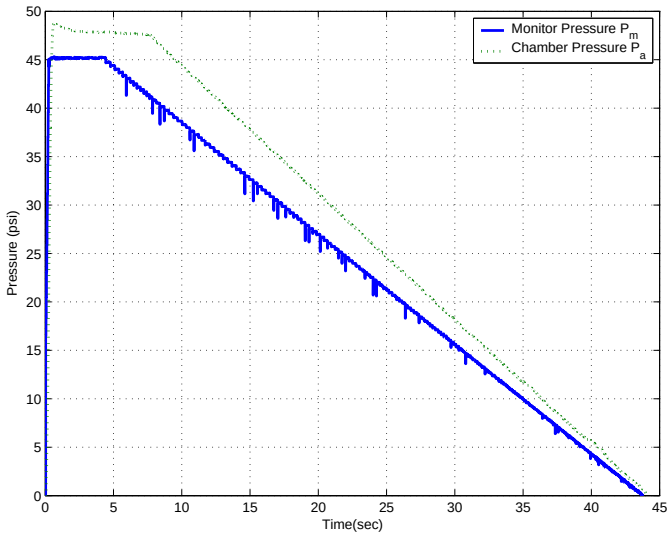

Fig. 7. Pressure response of ramp valve input for our experimental setup

following equation:

$$A_s(P_m, P_a) = k_s(r_s P_m - P_a) \qquad A_e(P_m, P_a) = k_e(P_a - r_s P_m) \tag{4}$$

where k_s and k_e are constants that can be determined, for example, based on the relationship in Fig. 7.

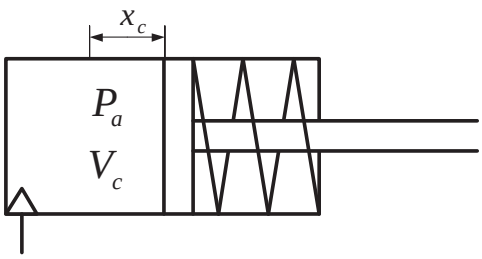

Fig. 8. Brake Chamber

B. Modeling of pneumatic brake

The brake chamber is a diaphragm-operated actuator which can be approximated by a single-acting pneumatic cylinder as shown in Fig. 8. $V_c(x_c)$ is the total air volume inside the brake

chamber and the pipe between the volume booster and the brake chamber; and $V_c(x_c)$ is a function of brake chamber stroke x_c. The pressure dynamics inside the brake chamber can be expressed by

$$\dot{P}_a V_c(x_c) + \gamma P_a \dot{V}_c(x_c) = \gamma \dot{m} R T \tag{5}$$

where the total volume $V_c(x_c) = V_d + A_c x_c$. V_d is the initial total dead volume before the brake is applied and A_c is the effective area of brake chamber. If we assume that the mass of the brake chamber push rod and brake chamber diaphragm can be neglected, the force balance on both side of the diaphragm can be described by:

$$k_r x_c = (P_a - P_{air})A_c - F_r \quad 0 \leq x_c \leq x_{cmax} \tag{6}$$

where k_r is the spring constant of the brake chamber return spring and F_r is the pre-load on the brake chamber return spring. The brake torque, T_b, acting on the wheel is proportional to the normal force acting on the brake pad

$$T_b = k_b((P_a - P_{air})A_c - F_r) \tag{7}$$

C. Modeling of vehicle motion during brake

A simple vehicle longitudinal braking dynamics can be described by [26]:

$$\begin{aligned} J_i \dot{\omega}_i &= R_i F_{bi}(\mu, \lambda_i, N_i) - T_{bi} - T_{tb} \\ M\ddot{x}_L &= -b\dot{x}_L - F_{da}(x_L^2) - \textstyle\sum_{i=1}^{n} F_{bi}(\mu, \lambda_i, N_i) \end{aligned} \tag{8}$$

where i indicates the wheel number, ω_i is the wheel angular velocity, R_i is the rotational radius of ith tire, F_{bi} is the braking force generated by the ith tire, T_{bi} is the brake torque acting on the ith tire, T_{tb} is the equivalent braking torque generated by vehicle engine/transmission, x_L is the longitudinal position, M denotes the vehicle mass, b is the viscous damping coefficient, $F_{da}(x_L^2)$ is the aerodynamic drag force which is a function of x_L^2, μ is the road surface friction coefficient, λ_i is the longitudinal slip of the ith wheel and N_i is the normal force at the ith wheel. The longitudinal slip λ_i is defined by $\lambda_i = \frac{\dot{x}_L - \omega_i R_i}{\dot{x}_L}$ when braking. The braking force $F_{bi}(\mu, \lambda_i, N_i)$ generated by ith tire is a highly nonlinear function of the road surface friction coefficient μ, tire longitudinal slip λ_i and normal force N_i.

D. Model reduction and validation

The proportional valve dynamics(1), the air flow equations (2-4), the chamber pressure dynamics equation (5), the brake torque generation equations (6-7), and the vehicle braking motion dynamics (8) represent accurate models of the pneumatic brake system and vehicle longitudinal motion during braking. They are rather complex for the controller design and many internal states are also difficult to measure (e.g. the brake chamber rod stroke x_c). Several steps of model reductions are made in this section to facilitate control design. Experimental data from the demonstration setup is presented to illustrate these model reductions.

In the chamber pressure equation (5), the brake chamber volume $V_c(x_c)$ is comprised of the initial dead volume V_d and the variable volume $A_c x_c$ from the chamber rod motion. The variable volume $A_c x_c$ is small enough to be neglected so that the volume $V_c(x_c)$ can be assumed to be a constant due to its short brake chamber stroke. Then Eq. (5) is reduced to:

$$\dot{P}_a = \frac{\gamma RT}{V_c}\dot{m} \tag{9}$$

Fig. 9- Fig. 11 show examples of comparisons between the experimental data from the demonstration setup and the simulation results of the simplified pneumatic brake system (Eqs. (1- 4) and Eq. (9)) for both the monitor pressure P_m and chamber pressure P_a using various types of inputs for proportional valve (Fig. 9: sine wave; Fig. 10: stair step; Fig. 11: ramp input). The results show a good match between the simulation results of simplified model and the experimental data. This validates the simplification from Eq. (5) to Eq. (9).

Aerodynamic drag force can be ignored due to slow speed of precision stopping application. During the precision stopping, the bus braking is usually kept smooth to ensure the passengers' comfort. Therefore, the longitudinal slip λ_i is generally small during this stopping process. It is therefore reasonable to assume that the braking force is proportional to the brake chamber pressure P_a. Fig. 12 shows experimental data between the brake chamber pressure and the bus deceleration for two different 40 foot CNG buses ($c1$ and $c2$). Although nonlinearities are dominant when chamber pressure is small, such a proportional assumption is good enough for the precision stopping control design when the brake pressure is, for the most part, sufficient large. Thus the brake torque generation equations (6-7) and the vehicle braking motion equation (8) can be simplified to:

$$M\ddot{x}_L = -F_b(P_a) - b\dot{x}_L \ , \quad F_b(P_a) = \zeta P_a + d \tag{10}$$

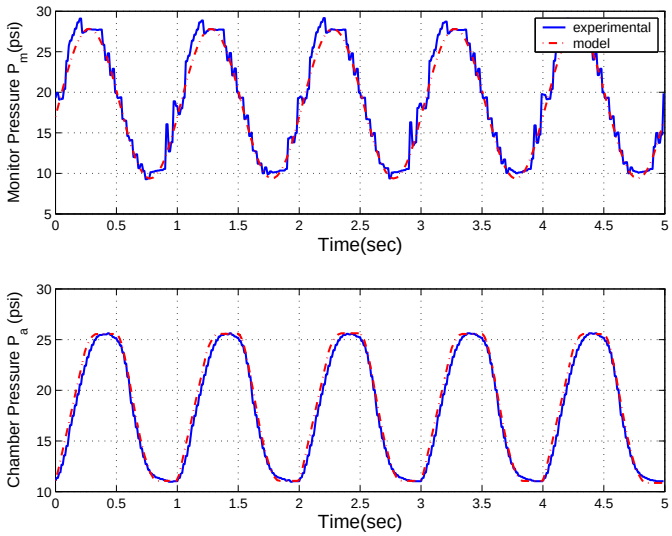

Fig. 9. Simulation Results of Simplified Model vs Experimental Data 1: sine wave input

where ζ and d are unknown constants. ζ represents the combined effect of road surface conditions, brake conditions (wear, temperature) and vehicle load. And d represents the combined effect of engine/transmission brake and road friction.

Since the bandwidth of the proportional pneumatic valve is far larger than the required bandwidth of longitudinal control for precision stopping, the proportional valve dynamics are neglected and the monitor pressure P_m is defined as the control input u for the following controller design and implementation. The control input in implementation, the proportional valve command input u_v, is related to the control input P_m by a known static gain.

IV. Controller Design

A. Problem formulation and design difficulties

Define the state variables $x = [x_1, x_2, x_3]^T = [x_L, \dot{x}_L, P_a]^T$, the simplified system model, Eqs. (2-4) and Eqs. (9-10), can be expressed in state-space form as

$$\begin{aligned} \dot{x}_1 &= x_2 \\ \dot{x}_2 &= -\frac{\zeta}{M}x_3 - \frac{b}{M}x_2 - \frac{d}{M} \\ \dot{x}_3 &= \frac{\gamma RT}{V_c}\dot{m}(x_3, u) \end{aligned} \tag{11}$$

where $\dot{m}(x_3, u)$ is the nonlinear flow mapping inside the pneumatic brake system defined by Eqs. (2)-(4) and $u = P_m$. The control objective is to synthesize a desired stopping trajectory $x_{1d}(t)$

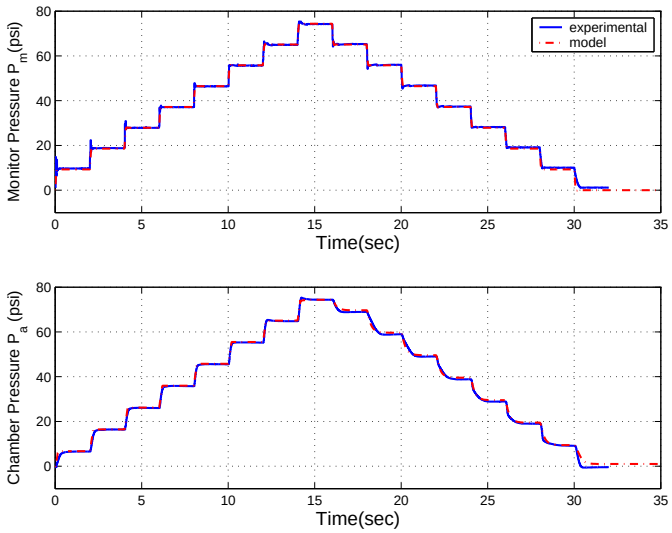

Fig. 10. Simulation Results of Simplified Model vs Experimental Data 2: step input

and a control input u such that the vehicle will follow the desired stopping trajectory and stop at the designated location with the desired accuracy ($e_{max} \leq 15cm$) and smoothness. In general, the system is subjected to parametric uncertainties due to the variations of M, ζ and d. In order to use parameter adaptation to reduce parametric uncertainties for an improved performance, the state-space equation (11) is linearly parametrized in terms of the unknown parameters. To achieve this, let $\theta = [\theta_1, \theta_2, \theta_3] = [\frac{\zeta}{M}, \frac{b}{M}, \frac{d}{M}]$; the state-space equation (11) is parametrized in terms of θ as:

$$\begin{aligned} \dot{x}_1 &= x_2 \\ \dot{x}_2 &= -\theta_1 x_3 - \theta_2 x_2 - \theta_3 \\ \dot{x}_3 &= \frac{\gamma RT}{V_c}\dot{m}(x_3, u) \end{aligned} \tag{12}$$

At this stage, it can be seen that the design difficulties associated with controlling the pneumatic system represented by Eq. (12) are:

- The pneumatic brake system is a highly nonlinear system. For example, Fig. 13 shows the chamber pressure responses in our experimental setup when the brake is applied and released. The apply response and release response are quite different. The nonlinearities come from the nonlinear pressure/flow relations described in Eqs. (2)-(4) and Eq. (9).
- The pneumatic brake system also has large model uncertainties. Examples of large model uncertainties include the vehicle load M and variation in ζ due to brake wear, temperature

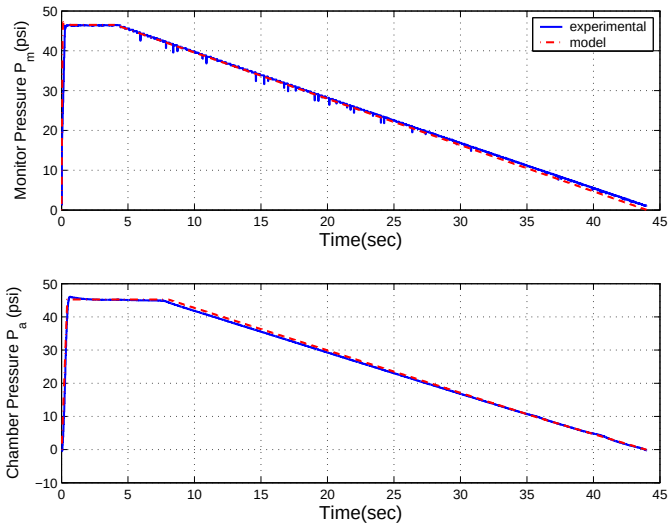

Fig. 11. Simulation Results of Simplified Model vs Experimental Data 3: ramp input

increase and change of road surface condition.

- The system has unmatched model uncertainties since model uncertainties appear in equations that do not contain control input u.
- As we found out in experimentation, strong feedback action usually introduces frequent brake apply-and-release. Such frequent apply-and-release brings several detrimental effects to the final performance. First, since the pressured air is released to the atmosphere when brake is releasing, frequent brake apply-and-release depletes supply air tank and lower supply air pressure. It will take a while for the system to recharge the supply air tank to its normal pressure when the supply pressure drops below certain threshold. Lower supply pressure slows already sluggish pneumatic dynamics. Second, frequent brake apply-and-release generates deceleration that makes passengers uncomfortable. Third, frequent brake apply-and-release also generates loud audible noise.
- The vehicle longitudinal position is calculated by combining the vehicle velocity and the vehicle position information from magnet markers or transbounders buried in the road surface, cameras with specific stripes on the road, or GPS receivers. However, magnet markers (which have approximately an 1 meter interval in our setup) or transbounders information is often discrete and the GPS signal may be blocked by architecture around the bus station. Furthermore, position dead reckoning with vehicle speed may not work at low

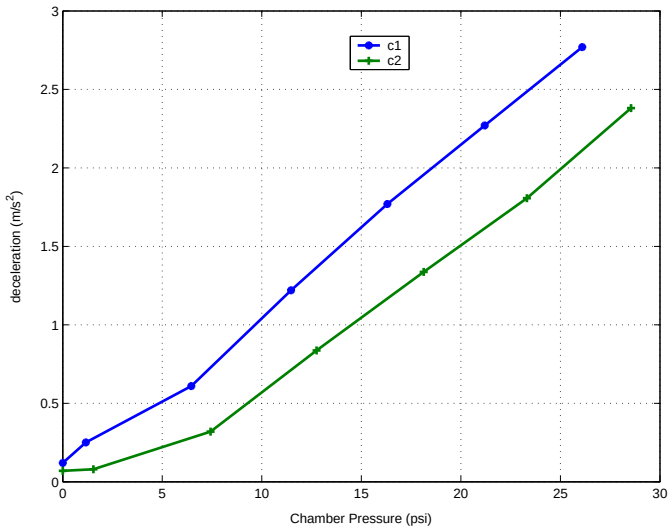

Fig. 12. Deceleration vs brake chamber pressure of two different CNG buses (c1 and c2)

speeds since most vehicle velocity sensors can only sense the velocity that is larger than the certain speed (e.g. $0.6m/s$ for our CNG buses). This means that the longitudinal velocity and position information for many precision stopping control system may not be available or accurate enough during the final phase of vehicle stopping when the accuracy needed to stop the vehicle is the most important. This paper also assumes this specific problem and designs a specific open loop control to deal with it.

To address the design difficulties mentioned above, the following strategies are adopted. First, a physical model-based nonlinear analysis and synthesis will be employed to address the nonlinear nature of the pneumatic brake system. Secondly, parameter adaptation will be adopted to reduce the effect of modeling uncertainties. Specifically, the Indirect Adaptive Robust Control (IARC) approach [19], [27]–[29] will be used to handle the general effects of model uncertainties. Third, the integrator backstepping design [29] via Lyapunov function will be used to address the mismatched model uncertainties. And lastly, the accurate parameter estimation from IARC parameters estimation will be used to calculate the open loop control command when longitudinal position information is not available at the final phase of vehicle stopping. Since the feedback control action is limited by the characteristics of pneumatic brake system, accurate parameter estimation is also important for the close loop control phase to provide accurate model compensation.

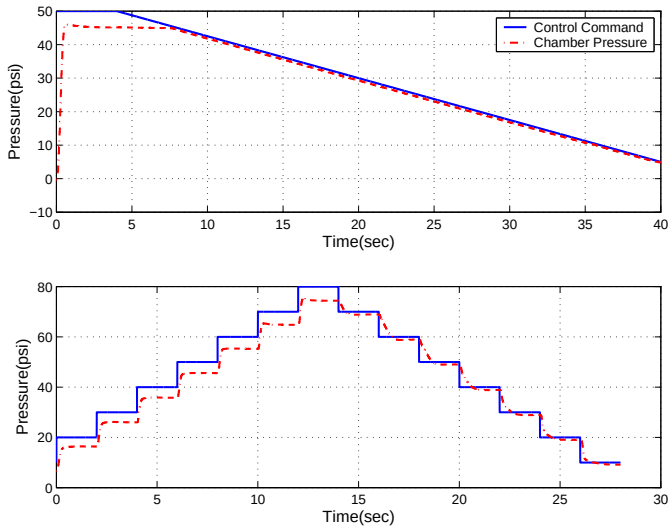

Fig. 13. Pneumatic brake system pressure response of experimental setup

B. Assumptions, notations and rate-limited adaptation law based on discontinuous projection mapping

For many applications, the extent of the parametric uncertainties are known. Thus, the following practical assumption is made:

Assumption 1: Parametric uncertainties satisfy:

$$\theta \in \Omega_\theta \triangleq \{\theta : \quad \theta_{min} < \theta < \theta_{max} \} \tag{13}$$

where θ_{min} and θ_{max} are known. ◇

Let $\hat{\theta}$ denote the estimations of unknown parameters θ and $\tilde{\theta} = \hat{\theta} - \theta$ represent the estimation error. In viewing Eq. (13), a simple discontinuous projection $Proj_{\hat{\theta}}$, can be defined as in [30], [31]:

$$Proj_{\hat{\theta}}(\bullet) = \begin{cases} 0 & \text{if } \hat{\theta} = \theta_{max} \text{ and } \bullet > 0 \\ 0 & \text{if } \hat{\theta} = \theta_{min} \text{ and } \bullet < 0 \\ \bullet & \text{otherwise} \end{cases} \tag{14}$$

A saturation function is defined as:

$$sat_{\dot{\theta}_M}(\Gamma\tau) = s_0\Gamma\tau, \qquad s_0 = \begin{cases} 1 & \|\Gamma\tau\| \leq \dot{\theta}_M \\ \frac{\dot{\theta}_M}{\|\Gamma\tau\|} & \|\Gamma\tau\| > \dot{\theta}_M \end{cases} \tag{15}$$

by using an adaptation law given by:

$$\dot{\hat{\theta}} = Proj_{\hat{\theta}}(sat_{\dot{\theta}_M}(\Gamma\tau)) \tag{16}$$

where $\Gamma > 0$ is a diagonal matrix, τ is an adaptation function to be synthesized later and $\dot{\theta}_M$ is the upper bound for the adaptation rate.

C. Controller design

Controller design consists of four parts: feedback controller design, open loop control design, parameter estimation design and the trajectory planning. The feedback controller design will employ the 2-step backstepping design technique presented in [19], [29], [32] based on the physical model of the pneumatic brake system represented by Eq. (12). Theoretical performance of the proposed controller and its proof can be found in Appendix.

1) ***Feedback Controller Design****:* The feedback controller is designed as follows: In the first step, chamber pressure x_3 will be treated as control input for the first two equations. A control function will be synthesized for x_3 for the design goal. In the second step, the real control input will be synthesized such that chamber pressure will track the control function we synthesized in the first step.

a) Backstepping step 1: Define a switching-function-like quantity as:

$$z_2 = x_2 - x_{2eq} = \dot{z}_1 + K_1 z_1 \qquad x_{2eq} = \dot{x}_{1d} - K_1 z_1 \tag{17}$$

where $z_1 = x_1 - x_{1d}$ is the output tracking error, x_{1d} is the desired trajectory to be tracked by x_1 and will be synthesized later, and K_1 is a positive constant feedback gain. Since $G_s(s) = z_1(s)/z_2(s) = 1/(s+K_1)$ is a stable transfer function, the reminder of the design is to make z_2 converge to zero. According to Eq. (12) and Eq. (17), the derivative of z_2 can be expressed by:

$$\dot{z}_2 = -\theta_1 x_3 - \theta_2 x_2 - \theta_3 - \dot{x}_{2eq} \qquad \dot{x}_{2eq} = \ddot{x}_{1d} + K_1 \dot{x}_{1d} - K_1 x_2 \tag{18}$$

It is clear from Eq. (18) that the brake chamber pressure x_3 can be treated as a virtual control input at this step. So the objective of this step is to synthesize a control function $P_{ad}(x_1, x_2, \hat{\theta}, t)$ for the virtual control input x_3 such that the output tracking error z_1 converges to zero. The resulting control function P_{ad} is given by:

$$\begin{aligned} &P_{ad} = P_{ada} + P_{ads} \\ &P_{ada} = \tfrac{1}{\hat{\theta}_1}(-\hat{\theta}_2 x_2 - \hat{\theta}_3 - \dot{x}_{2eq}) \\ &P_{ads} = P_{ads1} + P_{ads2} \quad , \; P_{ads1} = \tfrac{1}{\theta_{1min}} K_2 z_2 \end{aligned} \tag{19}$$

where P_{ada} is the model compensation part of the virtual control law, P_{ads} represents the feedback control part, and K_2 is a constant positive feedback gain. Let $z_3 = x_3 - P_{ad}$ denote the input discrepancy. From Eqs. (18-19), z_2 dynamics can be written as

$$\dot{z}_2 = -\theta_1 z_3 - \frac{\theta_1}{\theta_{1min}} K_2 z_2 - \theta_1 P_{ads2} + \phi_2^T \tilde{\theta} \tag{20}$$

where $\phi_2 = [P_{ada}, x_2, 1]^T$. The robust control part $P_{ads2} = \frac{1}{\theta_{1min}} K_{s2} z_2$ is now chosen to satisfy the following conditions

$$\begin{aligned} &\text{condition i} \qquad z_2[-\theta_1 P_{ads2} + \phi_2^T \tilde{\theta}] \leq \varepsilon_2 \\ &\text{condition ii} \qquad -z_2 P_{ads2} \leq 0 \end{aligned} \tag{21}$$

where K_{s2} is a positive control gain function and ε_2 is a positive design parameter. How to choose K_{s2} by satisfying the constraints similar to Eq. (21) can be found in [33]. Define a positive-semidefinite function $V_2 = \frac{1}{2} z_2^2$, its derivative can be written as:

$$\dot{V}_2 = -\frac{\theta_1}{\theta_{1min}} K_2 z_2^2 - \theta_1 z_2 z_3 + z_2[-\theta_1 P_{ads2} + \phi_2^T \tilde{\theta}] \tag{22}$$

b) Backstepping step 2: As seen from Eq. (22) in Step 1, if $z_3 = 0$, output tracking would be achieved by using the standard adaptive control argument in [29]. Therefore, Step 2 is to synthesize a control input so that z_3 either converges to zero or is bounded by a small value. From the system model equation (12), the z_3 dynamics can be written as:

$$\dot{z}_3 = \frac{\gamma RT}{V_c} \dot{m}(x_3, u) - \dot{P}_{ad} \tag{23}$$

where $\dot{P}_{ad} = \frac{\partial P_{ad}}{\partial x_1} x_2 + \frac{\partial P_{ad}}{\partial x_2} \dot{x_2} + \frac{\partial P_{ad}}{\partial \hat{\theta}} \dot{\hat{\theta}} + \frac{\partial P_{ad}}{\partial t}$. $\dot{P}_{ad}$ can be divided into two parts as shown in following equations:

$$\begin{aligned} \hat{\dot{P}}_{ad} &= \frac{\partial P_{ad}}{\partial x_1} x_2 + \frac{\partial P_{ad}}{\partial x_2} (-\hat{\theta}_1 x_3 - \hat{\theta}_2 x_2 - \hat{\theta}_3) + \frac{\partial P_{ad}}{\partial t} + \frac{\partial P_{ad}}{\partial \hat{\theta}} \dot{\hat{\theta}} \\ \tilde{\dot{P}}_{ad} &= \frac{\partial P_{ad}}{\partial x_2} (\tilde{\theta}_1 x_3 + \tilde{\theta}_2 x_2 + \tilde{\theta}_3) \end{aligned} \tag{24}$$

where $\hat{\dot{P}}_{ad}$ represents the calculable part which can be used in the design of control functions and $\tilde{\dot{P}}_{ad}$ is composed of various model uncertainties. From Eq. (23), the air flow rate to the brake chamber $\dot{m}$ can be treated as a virtual control input in Step 2. So Step 2 is to synthesize a control input $\dot{m}_d$ for $\dot{m}$ so that x_3 will track the desired control function P_{ad} that is synthesized in Step 1. Consider a p.s.d function $V_3 = V_2 + \frac{1}{2} z_3^2$, from Eqs. (22-23):

$$\dot{V}_3 = \dot{V}_2|_{P_{ad}} + z_3[\frac{\gamma RT}{V_c} \dot{m}(x_3, u) - \hat{\dot{P}}_{ad} - \hat{\theta}_1 z_2 - \phi_3^T \tilde{\theta}] \tag{25}$$

where $\dot{V}_2|_{P_{ad}}$ is a short-hand notation used to represent $\dot{V}_2$ when $x_3 = P_{ad}$ (or $z_3 = 0$) and $\phi_3 = [\frac{\partial P_{ad}}{\partial x_2} x_3 - z_2, \frac{\partial P_{ad}}{\partial x_2} x_2, \frac{\partial P_{ad}}{\partial x_2}]^T$. Using similar techniques, the control function $\dot{m}_d$ consists of the following two parts:

$$\begin{aligned} \dot{m}_d &= \dot{m}_{da} + \dot{m}_{ds} \\ \dot{m}_{da} &= \frac{V_c}{\gamma RT}(\hat{\dot{P}}_{ad} + \hat{\theta}_1 z_2) \\ \dot{m}_{ds} &= \dot{m}_{ds1} + \dot{m}_{ds2} \qquad \dot{m}_{ds1} = -\frac{V_c}{\gamma RT} K_3 z_3 \end{aligned} \tag{26}$$

where K_3 is a constant positive feedback gain. The time derivative of V_3 can be expressed by:

$$\dot{V}_3 = \dot{V}_2|_{P_{ad}} + z_3[\frac{\gamma RT}{V_c}\dot{m}_{ds2} - \phi_3^T\tilde{\theta}] - K_3 z_3^2 \tag{27}$$

The robust term $\dot{m}_{ds2} = -\frac{V_c}{\gamma RT} K_{s3} z_3$ can be chosen to satisfy following conditions:

$$\begin{aligned} &\text{condition i} \qquad z_3[\frac{\gamma RT}{V_c}\dot{m}_{ds2} - \phi_3^T\tilde{\theta}] \le \varepsilon_3 \\ &\text{condition ii} \qquad z_3\dot{m}_{ds2} \le 0 \end{aligned} \tag{28}$$

where ε_3 is a positive design parameter and K_{s3} is a positive control gain function. The control input u can be backed up from the nonlinear flow rate mapping equation (2) as:

$$u = \begin{cases} (\frac{\dot{m}_d}{k_s C_s P_s \sqrt{\frac{2}{RT}} f(\frac{x_3}{P_s})} + x_3)/r_s & \dot{m}_d \ge 0 (supply) \\ (\frac{\dot{m}_d}{k_e C_e x_3 \sqrt{\frac{2}{RT}} f(\frac{P_{air}}{x_3})} + x_3)/r_s & \dot{m}_d < 0 (release) \end{cases} \tag{29}$$

2) ***Open loop control****:* If vehicle velocity cannot be detected by the vehicle speed sensor when vehicle velocity is lower than a certain threshold (e.g. 0.6m/s for our CNG bus) at the final phrase of precision stopping and the position information is also not available or not accurate enough at the same time, the only sensor information available for feedback are the brake pressures. Precision stopping will enter the open loop control mode. For the open loop control, we assume that $x_1 = x_{1d}$ and $x_2 = \dot{x}_{1d}$ (i.e. $z_1 = z_2 = 0$) and the parameter adaptation is also frozen, i.e. $\dot{\hat{\theta}} = 0$.

3) ***Adaptation law design****:* In order to use an indirect parameter adaptation based on x-swapping [19], [29], [34], it is desirable to obtain a static model for the prediction error that is based on the state x and is linearly parameterized in terms of the parameter estimation error. Since the parametric uncertainties exist only in the second equation in the system model (12) and the vehicle acceleration measurement $\dot{x}_2$ is either not available or too noisy, a first order filter is added to transfer the dynamic relationship to a static relationship:

$$x_2 - \frac{a}{s+a}x_2 = \theta_1(-\frac{1}{s+a}x_3) + \theta_2(-\frac{1}{s+a}x_2) + \theta_3(-\frac{1}{s+a}) \qquad a > 0 \tag{30}$$

where a is a positive constant. Define $y = x_2 - \frac{a}{s+a}x_2$ and $\Omega = [-\frac{1}{s+a}x_3, -\frac{1}{s+a}x_2, -\frac{1}{s+a}]^T$, and then the static relationship can be expressed by:

$$y = \Omega^T \theta \tag{31}$$

Define the estimation of y as $\hat{y} = \Omega^T \hat{\theta}$ and the model prediction error $\eta = \hat{y} - y = \Omega^T \tilde{\theta}$, and then various estimation algorithms can be applied. For the gradient method, the parameter estimations are updated by:

$$\dot{\hat{\theta}} = Proj_{\hat{\theta}}(sat_{\dot{\theta}_M}(-\Gamma \frac{\Omega \eta}{1+\nu Trace(\Omega^T \Omega)})) \tag{32}$$

where $\Gamma = diag\{\gamma_1, \gamma_2, \gamma_3\}$ is a positive constant adaptation gain matrix, and ν is a non-negative constant.

For the least square method, the parameter estimations are updated by:

$$\dot{\hat{\theta}} = Proj_{\hat{\theta}}(sat_{\dot{\theta}_M}(-\Gamma \frac{\Omega \eta}{1+\nu Trace(\Omega^T \Gamma \Omega)}) \tag{33}$$

where Γ is updated by:

$$\dot{\Gamma} = \alpha \Gamma - \frac{\Gamma \Omega \Omega^T \Gamma}{1+\nu Trace(\Omega^T \Gamma \Omega)} \tag{34}$$

where $\alpha \geq 0$ is the forgetting factor.

4) ***Trajectory planning****:* A polynomial trajectory is synthesized for the smooth stop of a heavy-duty vehicle. The trajectory should satisfy the following boundary conditions:

$$\begin{aligned} x_{1d}(0) &= 0 \quad & x_{1d}(T) &= P_0 \\ \dot{x}_{1d}(0) &= v_0 \quad & \dot{x}_{1d}(T) &= 0 \\ \ddot{x}_{1d}(0) &= 0 \quad & \ddot{x}_{1d}(T) &= 0 \end{aligned} \tag{35}$$

where T is the time when the vehicle fully stops and P_0 is the distance from where the vehicle begins precision stopping to its final stopping point. Assume that:

$$x_{1d}(t) = a_5 t^5 + a_4 t^4 + a_3 t^3 + a_2 t^2 + a_1 t + a_0 \tag{36}$$

The coefficients of the trajectory can be solved as:

$$\begin{aligned} a_0 &= 0 & a_1 &= v_0 & a_2 &= 0 \\ a_3 &= \tfrac{10P_0 - 6v_0 T}{T^3} & a_4 &= \tfrac{8v_0 T - 15P_0}{T^4} & a_5 &= \tfrac{6P_0 - 3v_0 T}{T^5} \end{aligned} \tag{37}$$

T can be adjusted to accommodate the passenger comfort requirements while stopping.

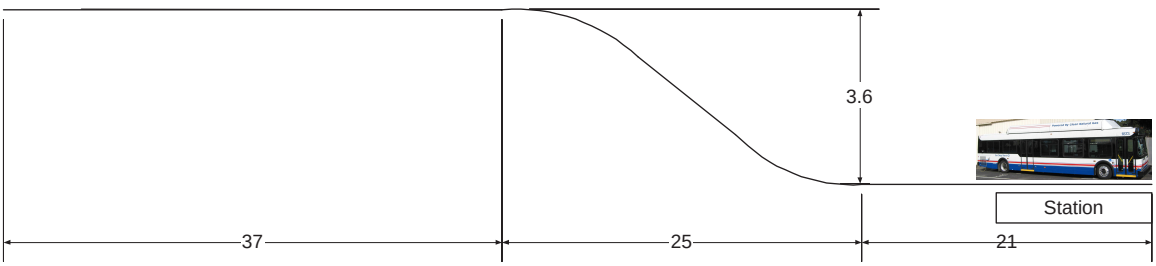

Fig. 14. Docking Demo in Washington DC

V. Experimental results

A. Precision Docking Demo scenario and system configuration

Fig. 14 shows the docking track configuration of the Washington DC docking demo during June 24-26, 2003. The whole docking demo procedure is described as follows from the longitudinal control point of view. The demo bus starts manually by the driver. The driver could select the manual or automatic transition to the automatic control mode anytime he chooses. Once switched to the automatic control mode, the bus will automatically slow down or speed up to a predetermined cruising speed. When the bus reaches at the location which is 12.0 meters to the designated final stopping point, it starts the precision stopping process and stops exactly at the predetermined position along the station.

Two New Flyer 40 footer CNG buses (c_1 and c_2) are retrofitted for the precision docking maneuver as shown in Fig 15. Magnetometer sensors are installed under the bus to detect magnets buried in the road with a meter spacing. The magnets provide both lateral and longitudinal positions. The throttle is modified so that it can be controlled through a computer. The original pneumatic brake system is retrofitted as shown in Fig. 3. ”Off-the-Shelf” products, Proportion-Air’s QB1 proportional pneumatic valve and Proportional-Air R series volume booster, are used for the brake actuator. Pressure sensors are installed to measure internal pressures (monitor pressure P_m and chamber pressure P_a) of the brake actuator and the pneumatic brake system. The internal vehicle data network (J1939 bus) of the CNG bus is tapped to receive information on the engine and transmission states, such as vehicle speed, engine speed and gear position, which is broadcasted by the engine and transmission Electrical Control Unit (ECU). The lowest speed that measures by the wheel speed sensor is about $0.6m/s$. Continuous longitudinal position

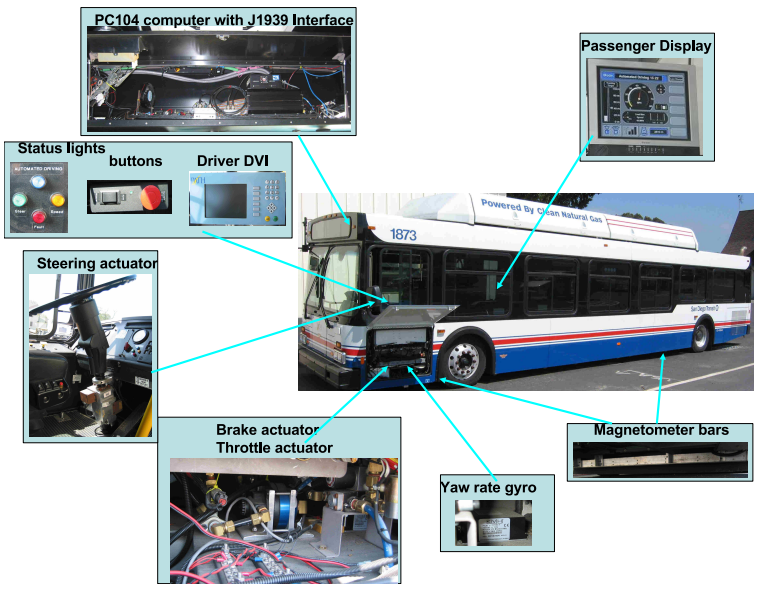

Fig. 15. New Flyer CNG 40 footer bus configuration

is available by integrating the last magnet position and vehicle speed. Control program is running in a on-board PC104 computer under the QNX real-time operating system.

B. Parameters of the Precision Stopping Controller

The precision stopping controller represented by Eq. (29) and Eq. (16) is executed at $50Hz$ sampling frequency. For the feedback controller part, the robust control gain functions K_{s2} and K_{s3} are chosen as in [33] to satisfy the constraints in Eq. (21) and Eq. (28):

$$K_{s2} \geq \frac{1}{2\varepsilon_2}\|\theta_M\|^2\|\phi_2\|^2 \qquad K_{s3} \geq \frac{1}{2\varepsilon_3}\|\theta_M\|^2\|\phi_3\|^2 \tag{38}$$

where $\theta_M = \theta_{max} - \theta_{min}$, $\varepsilon_2 = 4.5$ and $\varepsilon_3 = 11.0$. The following parameters are used for constant feedback gains in Eq. (17), Eq. (19) and Eq. (26): $K_1 = 8.5$, $K_2 = 7.5$ and $K_3 = 7.5$. For the parameter estimation, the least square method in Eq. (33-34) is chosen and parameters a, α and ν are chosen as: $a = 25$, $\alpha = 0.8$ and $\nu = 1.0$. Initial parameter estimation gains $\Gamma(0)$ are chosen as $\Gamma(0) = \mathbf{diag}\{25, 10, 35\}$. The upper limits θ_{max} and the lower limits θ_{min} of the unknown parameters θ in Eq. (13) are chosen as: $\theta_{max} = [0.6, 0.15, 1.2]^T$ and $\theta_{min} = [0.15, 0.04, 0.2]^T$. Since the starting velocity v_0 is regulated around $3.1m/s$ by the throttle control and the braking distance is chosen to be $P_0 = 12.0m$, stopping time $T = \frac{2P_0}{v_0}$ is selected.

C. Experimental results from Washington DC Demonstration

As one of precision docking's functions, precision stopping was demonstrated publicly at Washington DC during June 24-26, 2003 [35]. There were about 15-18 runs each day. Passenger counts ranged from 1 or 2 to a full bus load. The demonstration was also performed under rainy conditions. The final stopping accuracy was consistently controlled under 15*cm* with the desired stopping smoothness, without a single failure for over 50 total demonstration runs. Data from three different scenarios in the demonstration are shown in the following figures to illustrate the effectiveness and robustness of the designed control algorithm. They are: bus with full load on dry road, empty bus on dry road and almost empty bus on wet road. To illustrate the effectiveness of parameter estimation, the experimental result of empty bus on wet road without parameter estimation (i.e. $\Gamma = \mathbf{diag}\{0,0,0\}$) is also shown in the following figures. Fig. 16 shows the

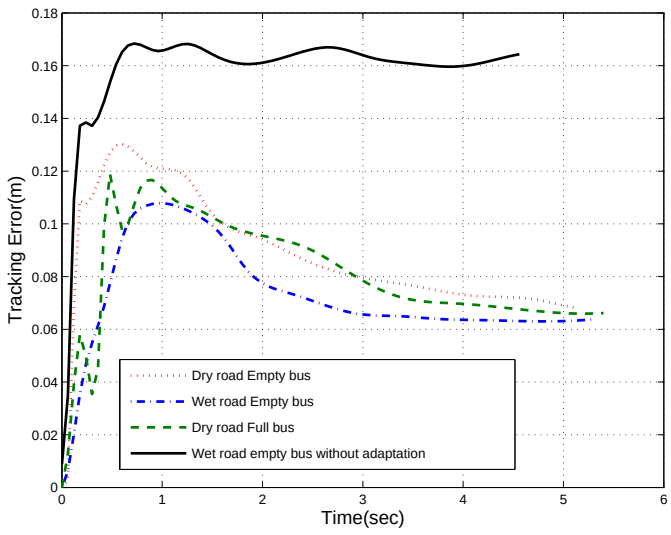

Fig. 16. Tracking error for 3 different scenarios

tracking error for the 4 different scenarios before longitudinal position information becomes unavailable just before the final stop. Final stopping errors are measured manually when the bus is fully stopped and they are well kept within a 15*cm* accuracy bound for the cases with parameter estimation. For the case without parameter estimation, the final stopping error is larger than 30*cm*. Testing experiences reveal that a good estimation of θ_1, the combined effects of bus load, brake characteristics and road surface condition, is very important to the final stopping accuracy. Fig. 17 shows the parameter estimation for θ_1. As shown in Fig. 16 and 17, tracking

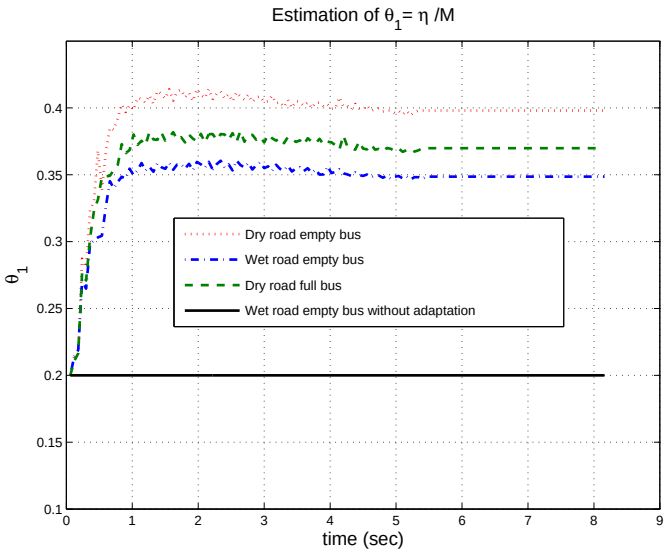

Fig. 17. Estimation of θ_1 for 3 different scenarios

errors increase when the vehicle starts braking; at the same time, θ_1 estimations are also far away from their true values. As θ_1 estimation converges, tracking errors are also reduced. Generally about 5.1-5.2 sec after the control starts and when the bus has almost stopped, the longitudinal position and velocity measurement is no longer available and the parameter estimation is frozen. The vehicle then begins entering the final open loop braking control phase. Because of the accurate parameter estimations, the system is able to maintain a final stopping accuracy better than 15cm with 2 to 4 seconds open loop control at extremely low speeds. The experimental results also show that the parameter estimation also helps reduce tracking error in the close loop control phase.

VI. Conclusion

This paper focuses on the precision stopping control problem for heavy-duty vehicles equipped with a pneumatic brake system. It is a control application paper that integrates various control synthesis tools to solve a real-world control problem. The design process includes system modeling, model reduction, control synthesis, implementation and successful public demonstration. The paper starts with a detailed model and the appropriate model reduction of the pneumatic brake system with an actuator. The IARC controller is then constructed based on the reduced pneumatic brake system model. The controller is chosen because it can take into

account particular nonlinearities and large uncertainties in the heavy-duty vehicle environment. An Indirect Adaptive Control design technique is used to decouple the feedback control design from the parameter estimation design. This method improves the accuracy of the unknown parameter estimation which is crucial for maintaining the final stopping accuracy when it is possible that the sensor information on the vehicle velocity and position can become unavailable just before the vehicle is fully stopped. This precision stopping control design was implemented on two 40-foot CNG buses and was demonstrated at a precision docking demonstration in Washington DC during June 24-26, 2003. The successful 3-day public demonstration showcased the smooth stopping performance with consistent 15cm stopping accuracy under different operational conditions without a single failure. Experimental data from the demonstration further illustrated the effectiveness and robustness of the proposed controller design.

APPENDIX

Theorem 1: The following results hold that if the control law (29) with any rate-limited projection-type adaptation law (16) (e.g. gradient type estimator (32) or least square type estimator (33)) are applied:

A. The tracking errors $z = [z_1, z_2, z_3]^T$ are generally bounded. Furthermore, $V_3 = \frac{1}{2}(z_2^2 + z_3^2)$, an index for the bound of the tracking error z, is bound above by

$$V_3(t) \quad \leq exp(-\lambda_V t)V_3(0) + \frac{\varepsilon_V}{\lambda_V}[1 - exp(-\lambda_V t)] \tag{39}$$

where $\lambda_V = 2min\{K_2, K_3\}$ and $\varepsilon_V = \varepsilon_2 + \varepsilon_3$. The output tracking error $z_1 = x_1 - x_{1d}(t)$ can be guaranteed to have prescribed transient performance by suitably selecting certain controller parameters.

B If the following persistent exciting condition is satisfied:

$$\int_t^{t+T_0} \Omega\Omega^T d\tau \geq KI \qquad K > 0 \qquad T_0 > 0 \tag{40}$$

the parameter estimations $\hat{\theta}$ converge to their true values (i.e. $\tilde{\theta} \to 0$ as $t \to \infty$) and asymptotic tracking is also achieved (i.e. $z \to 0$ as $t \to \infty$)

Proof :

A .From (22) and (27), $\dot{V}_3$ can be written as

$$\dot{V}_3 = -\frac{\theta_1}{\theta_{1min}} K_2 z_2^2 - K_3 z_3^2 + z_2(-\theta_1 P_{ads2} + \phi_2^T \tilde{\theta}) + z_3(\frac{\gamma RT}{V_c}\dot{m}_{ds2} - \phi_3^T \tilde{\theta}) \tag{41}$$

From condition i of (21) and (28), (41) becomes

$$\dot{V}_3 \leq -K_2 z_2^2 - K_3 z_3^2 + \varepsilon_2 + \varepsilon_3 \leq -\lambda_V V_3 + \varepsilon_V \tag{42}$$

which leads to the results A in Theorem 1

B .Detailed proof of part B for a more general SISO nonlinear systems in semi-strict feedback forms can be found in [19] □

REFERENCES

[1] P. A. Ioannou, Ed., *Automated Highway Systems*. Kluwer Academic/Plenum Publishers, 1997.

[2] R. G. Hebden, C. Edwards, and S. K. Spurgeon, "Automotive steering control in a split-mu manoeuvre using an observer-based sliding mode controller," *Vehicle System Dynamics*, vol. 41, no. 3, pp. 181–202, 2004.

[3] "Intelligent vehicle initiative needs assesment," Federal Transit Administraion, Tech. Rep. FTA-TRI-11-99-33, 1999.

[4] R. Bishop, "Intelligent vehicle applications worldwide," *IEEE Intelligent Systems*, vol. 15, no. 1, 2000.

[5] M. Donath, C. SHankwitz, L. Alexander, A. Gorjestani, P. Cheng, and B. Newstrom, "Bus rapid transit lane assist technology systems," University of Minnesota, Tech. Rep., 2003.

[6] P. A. Ioannou, H. Jula, C. Liu, K. Vukadinovic, and H. Pourmohammadi, "Advanced material handeling: Automated guided vehicles in agile ports," University of Southern California, Tech. Rep., 2000.

[7] H.-S. Tan, "An automated snowblower for highway winter operation," *Intellimotion*, vol. 10, no. 4, pp. 1–2, 2004.

[8] R. Rajamani, S. B. Choi, B. K. Law, J. K. Hedrick, R. Prohaska, and P. Kretz, "Design and experimental implementation of longitudinal control for a platoon of automated vehicles," *Transactions of ASME, Journal of Dynamic Systems, Measurement, and Control*, vol. 122, no. September, pp. 470–476, 2000.

[9] D. Yanakiev and I. Kanellakopoulos, "Longitudinal control of automated chvs with significant acutator delays," *IEEE Transactions on Vehicular Technology*, vol. 50, no. 5, pp. 1289–1297, 2001.

[10] C. Liang and H. Peng, "Optimal adaptive cruise control with guaranteed string stability," *Vehicle System Dynamics*, vol. 32, no. 4, pp. 313–330, 1999.

[11] D. Swaroop and J. K. Hedrick, "String stability of interconnected systems," *IEEE Transactions on Automatic Control*, vol. 41, no. 3, pp. 349–357, 1996.

[12] C. Hatipoglu, Y. Hai, and U. Ozguner, "Self-optimizing brake control design for commercial vehicles," in *SAE Technical Paper*, no. 2001-01-2731, 2001.

[13] P. Heinzl, P. Lugner, and M. Plochl, "Stability control of a passenger car by combined additional steering and unilateral braking," *Vehicle System Dynamics*, vol. 37, no. SUPPL., pp. 221–233, 2003.

[14] S. B. Choi and P. Devlin, "Throttle and brake combined control for intelligent vehicle highway systems," in *SAE Technical Paper*, no. 951897, 1995.

[15] T. Acarman, U. Ozguner, C. Hatipoglu, and A. Lgusky, "Pneumatic brake system modeling for systems analysis," in *SAE Technical Paper*, no. 2000-01-3414, 2000.

[16] S. C. Subramanian, S. Darbha, and K. Rajagopal, "Modeling the pneumatic subsystem of a s-cam air brake system," *Transactions of ASME, Journal of Dynamic Systems, Measurement, and Control*, vol. 126, no. 1, pp. 36–46, 2004.

[17] X. Lu and J. Hedrick, "Longitudinal control design and experiment for heavy-duty trucks," in *Proc. of 2003 American Control Conference*, 2003, pp. 36–41.

[18] J. Bobrow and B. McDonell, “Modeling, identification, and control of a pneumatically actuated, force controllable robot,” *IEEE Transactions on Robotics and Automation*, vol. 14, no. 5, pp. 732–742, 1998.

[19] B. Yao, “Integrated direct/indirect adaptive robust control of siso nonlinear systems in semi-strict feedback form,” in *American Control Conference*, 2003, pp. 3020–3025.

[20] F. Bu and B. Yao, “Integrated direct/indirect adaptive robust motion control of single-rod hydraulic actuators with time-varying unknown inertia,” in *Proc. of IEEE/ASME International Conference on Advanced Intelligent Mechatronics (AIM)*, Italy, 2001.

[21] L. L. Hoberock, “A survey of longitudinal acceleration comfort studies in ground transportation vehicle,” *ASME J. of Dynamic Systems, Measurement, and Control*, vol. 99, no. 2, pp. 76–84, 1977.

[22] W. C. Caywood, H. L. Donnelly, and N. Rubinstein, “Guideline for ride-quality specifications based on transpo ’72 test data,” Applied Physics Laboratory, The Johns Hopkins University, Tech. Rep. APL/JHU CP 060/TPR 039, 1977.

[23] L. Alexander and M. Donath, “Differential gps based control of a heavy vehicle,” University of Minnesota, Twin City, Tech. Rep. 2000-05, 2000.

[24] S. R. Dickey and X. Y. Lu, “Control actuation of fully automated heavy-duty vehicles using sae j1939,” in *Proc. IEEE Intelligent Vehicles Symposium (IV2003)*, 2003, pp. 400–405.

[25] P. Bigras and K. Khayati, “Nonlinear observer for pneumatic system with non negligible connection port restriction,” in *American Control Conference*, Anchorage, AK, 2002, pp. 3191–3195.

[26] K. Lee, J. Jeon, D. Hwang, and Y. Kim, “Performance evaluation of antilock brake controller for pneumatic brake system,” in *Proc. IEEE Industry Applications Conference*, vol. 1, 2003, pp. 301–307.

[27] B. Yao and M. Tomizuka, “Smooth robust adaptive sliding mode control of robot manipulators with guaranteed transient performance,” in *Proc. of American Control Conference*, Green Valley, AZ, 1994, pp. 1176–1180, the full paper appeared in *ASME Journal of Dynamic Systems, Measurement and Control*, Vol. 118, No.4, pp764-775, 1996.

[28] B. Yao, “High performance adaptive robust control of nonlinear systems: a general framework and new schemes,” in *Proc. of IEEE Conference on Decision and Control*, San Diego, CA, 1997, pp. 2489–2494.

[29] M. Krstic, I. Kanellakopoulos, and P. V. Kokotovic, *Nonlinear and adaptive control design*. New York: Wiley, 1995.

[30] S. Sastry and M. Bodson, *Adaptive Control: Stability, Convergence and Robustness*. Englewood Cliffs, NJ 07632, USA: Prentice Hall, Inc., 1989.

[31] G. C. Goodwin and D. Q. Mayne, “A parameter estimation perspective of continuous time model reference adaptive control,” *Automatica*, vol. 23, no. 1, pp. 57–70, 1989.

[32] B. Yao, F. Bu, J. Reedy, and G. Chiu, “Adaptive robust control of single-rod hydraulic actuators: theory and experiments,” *IEEE/ASME Trans. on Mechatronics*, vol. 5, no. 1, pp. 79–91, 2000.

[33] B. Yao and M. Tomizuka, “Adaptive robust control of SISO nonlinear systems in a semi-strict feedback form,” *Automatica*, vol. 33, no. 5, pp. 893–900, 1997.

[34] B. Yao and A. Palmer, “Indirect adaptive robust control of siso nonlinear systems in semi-strict feedback form,” in *IFAC World Congress*, 2002, pp. 1–6.

[35] C.-Y. Chang, J. Misener, and J. Lins, “Smart buses, smart intersection shine at washington ivi meeting,” *Intellimotion*, vol. 10, no. 3, pp. 2–3, 2003.